Journal of Science: Advanced Materials and Devices 6 (2021) 209–214

Contents lists available at ScienceDirect

Journal of Science: Advanced Materials and Devices

journal homepage: www.elsevier.com/locate/jsamd

Original Article

Heterostructure of TiO_2 and macroporous silicon: The simplest relaxation oscillator

Abel Garzon-Roman [a], Enrique Quiroga-González [b, *], Carlos Zúñiga-Islas [a, **]

[a] National Institute for Astrophysics, Optics and Electronics (INAOE), 72840, Santa Maria Tonantzintla, Mexico
[b] Institute of Physics, Benemérita Universidad Autónoma de Puebla, San Claudio and 18 Sur, Building IF-1, 72570, Puebla, Mexico

ARTICLE INFO

Article history:
Received 30 December 2020
Accepted 13 January 2021
Available online 19 January 2021

Keywords:
TiO_2
Porous silicon
Relaxation oscillator
Tunnel diode effect
Temporal oscillations

ABSTRACT

A heterostructure composed of TiO_2 and macroporous silicon in this study may represent the simplest relaxation oscillator ever reported. It consisted of macroporous Si with TiO_2 grown on its pore walls, and metallic contacts. This is also the first relaxation oscillator of its kind. Such oscillators are commonly formed by a capacitor or an inductor and a feedback loop with a switching device operating with a threshold voltage. The dielectric characteristics of TiO_2 (capacitive behavior) in combination with the tunnel diode characteristics of the heterostructure (presenting a negative differential resistance, when activated at a threshold voltage) are shown to give rise to the relaxation oscillations.

1. Introduction

The attractive properties of TiO_2 make it one of the most important semiconductors for multiple applications, in electronics, sensing, catalysis, etc. Structures of TiO_2 can be obtained by different methods, such as atomic layer deposition (ALD) [1], pulsed laser deposition [2], chemical beam epitaxy [3], sol–gel [4], solvothermal synthesis [5], and more [6,7]. TiO_2 has been used as an electrode for high electron injection, improving efficiencies of solar cells [8]. Moreover, TiO_2 has a high dielectric constant (k~80) [8]. This material is also transparent to visible light, showing a very high optical transmittance [1]. These characteristics have been very useful in different microelectronic and nanoelectronic applications, such as dielectric in storage capacitors in DRAM and nonvolatile memories [9]. Nano-fabrication of this material has demonstrated different properties that have been attributed to quantum effects [1].

Heterostructures of TiO_2 with Si have been used to develop devices that are compatible with the microelectronic industry (mainly based on Si). Such structures present p–n junctions, which are important to separate charges, e.g. for photocatalysis [10], solar cells [11], or photodetectors [12], to mention some applications. However, looking for new effects, porous Si (por-Si) has been substituting bulk Si in many devices. This material can be used as support [13], with porosities ranging from micro- (pore diameters below 2 nm) to macro-porosity (pore diameters more significant than 50 nm), which can be modulated in-depth [14]. The porosity represents a higher surface area than bulk Si, allowing the faster mass transfer [15]. Additionally, due to the pore walls' defect-rich surface, it has open bonds that can be easily functionalized and could act as nucleation centers to grow other materials and to form composites. Furthermore, this material exhibits optical and electronic bandgaps that can be tuned with the degree of porosity and/or level of defects. Taking advantage of these properties, heterostructures of TiO_2 with por-Si, presenting novel or enhanced properties have been developed: enhanced photocatalytic activity [16,17], enhanced fluorescence for sensing [18], enhanced adsorption of gases [19], enhanced light absorption [20], thermoelectric properties [21], etc. However, in the most of the cases, the authors do not take full advantage of the pore wall surface properties, since just in a few works the deposition of TiO_2 went inside the pores (mostly using ALD) [16,18].

In the present work, novel heterostructures consisting of por-Si with TiO_2 grown inside its pores are produced, and their electrical responses are reported. In the literature, there is limited information about the electrical properties of such heterostructures. This could arise due to the difficulties encountered to produce them,

* Corresponding author.
** Corresponding author.
E-mail addresses: equiroga@ieee.org (E. Quiroga-González), czuniga@inaoep.mx (C. Zúñiga-Islas).
Peer review under responsibility of Vietnam National University, Hanoi.

https://doi.org/10.1016/j.jsamd.2021.01.003

usually requiring sophisticated equipment like ALD. Herein, the solvothermal route (a straightforward and cheap chemical approach) has been used to produce the heterostructures. Their resulting electrical properties are unique and presented for the TiO_2/Si system for the first time: relaxation oscillations. There are no other devices utilizing this class of material presenting such an effect, not even complex nano-devices [22]. A thorough analysis of the phenomenon is presented in this work.

2. Materials and methods

In Fig. 1, the structure of a device is depicted. It consists of por-Si with TiO_2 nanoparticles grown on its pore-walls, and with Ni and Al contacts. The por-Si matrix was prepared by metal-assisted chemical etching (MACE) using (100) Si wafers with a resistivity of 15–25 Ωcm. Ag particles have been chemically deposited on Si by immersing the wafers in aqueous solutions of $AgNO_3$ and HF. The metallic particles served as the catalyst for the production of pores, in aqueous solutions of H_2O_2 and HF. The whole process has been fully described in a previous work of the authors [23]. After the chemical etching, the wafers were rinsed with deionized water and dried with nitrogen flow.

TiO_2 was deposited inside and above the porous structure of Si by the solvothermal route, at 180 °C, in Teflon-lined stainless steel autoclaves, for 4 h. The filling volume was about 80%. Titanium butoxide (TiBu) was used as the precursor, hydrochloric acid (HCl) was used to produce an acidic medium, and ethylene glycol (EtGl) was employed as a solvent. Three different composites were obtained varying the volume proportion of the substances (TiBu: HCl: EtGl): 2:1:10 (for the sample "high") 1:4:10 (for "medium"), and 1:6:10 (for "low"). After rinsing with acetone and deionized water, the samples were dried with nitrogen flow, and then were thermally treated at 400 °C for 3 h under air.

To perform electrical characterization, Ni circular contacts (with a diameter of 1 mm and thickness of 500 nm) were deposited on the top of the heterostructures. In contrast, a single whole area Al contact was deposited on the backside of the heterostructures (with a thickness of 500 nm) by high vacuum metal evaporation.

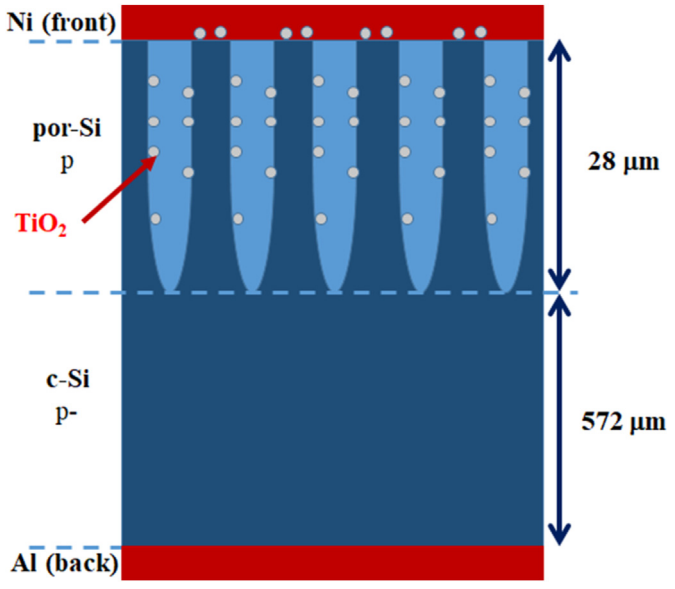

Fig. 1. Schematic of a TiO_2/por-Si heterostructure studied in this work. The upper elongated figures represent the pores in Si (forming por-Si).

Finally, the heterostructures were thermally treated at 400 °C for 30 min under N_2 flow in order to improve the adherence of the metal contacts.

The samples were characterized by Field-Emission Scanning Electron Microscopy (FE-SEM) FEI-SCIOS DualBeam. Current–voltage (I–V) and current–time (I-t) characteristics were measured with a Keithley 4200A-SCS Parameter Analyzer. The I–V curves were recorded from negative to positive voltages at a voltage sweep rate of 1.4 V/s. The current was limited to 10 mA to avoid damaging the devices.

3. Results and discussion

3.1. Structure and electronic transport in macroporous Si on bulk Si

To understand the contribution of porous Si (por-Si) to the TiO_2/por-Si heterostructures, it was analyzed before the deposition of TiO_2. Fig. 2a shows the SEM micrograph of the surface of por-Si. It presents a structure similar to the one of macroporous Si prepared electrochemically without defined patterns. The cross-section of the pores is quasi-circular. The pores are homogeneously distributed, with an average pore diameter of about 60 nm. The shape, size, and distribution of the pores depend directly on the Ag particles deposited for the MACE etching process, whose deposition mechanism depends on the plating solutions and doping of the Si substrate [24]. The por-Si section has a depth of around 28 μm. Underneath this section, a thick c-Si (bulk crystalline Si) section is found (see the schematic of Fig. 1).

Electrical contacts were deposited to characterize the electrical properties of the por-Si/c-Si heterojunction in the same way as the whole heterostructures with TiO_2 (see section 4). From the I–V characteristics shown in Fig. 2b, it can be seen that the transport is asymmetric with respect to polarization, with small activation energy of 70 meV for reverse polarization. However, the structure conducts electricity in both polarizations, in contrast to a typical rectifying diode. This behavior has been reported for mesoporous Si/c-Si heterojunctions, with defects cured by an H_2 treatment [25]. In the present case, the amount of defects is not as high as in mesoporous Si produced electrochemically (sponge-like); these defects do not represent traps, but increase the number of available carriers in comparison to c-Si (a low doped material), producing the small barrier for reverse polarization. Fig. 2c shows the energy band diagram of the heterojunction. The bandgap of por-Si has been considered 1.64 eV, as the optical bandgap is estimated in the previous work [23]. This value is close to the value of about 1.8 eV reported for electrochemically prepared por-Si with similar porosity [26,27]. Due to the higher availability of charges in por-Si, this material is considered p, as compared to the substrate, which is p-. It is important to mention that the junction's energy barrier does not represent an important practical impediment for electrical transport, since it is not much higher than the thermal energy at room temperature (about 26 meV).

3.2. Structure and electronic transport in TiO_2/macroporous Si heterostructures (tunnel diode – like behavior)

Figure 3 shows cross-sectional SEM micrographs of the three different TiO_2/por-Si heterostructures. In all cases, TiO_2 particles are grown on the pore walls of por-Si; however, the spatial density of particles decreases with the amount of TiBu used for the synthesis: density of "high" < density of "medium" < density of "low". This occurs because with larger concentrations of the precursor, the reaction rate increases dramatically, and takes place more on the surface of por-Si than inside the pores (limited diffusion process). Reducing the reactant concentration, the deposition rate starts

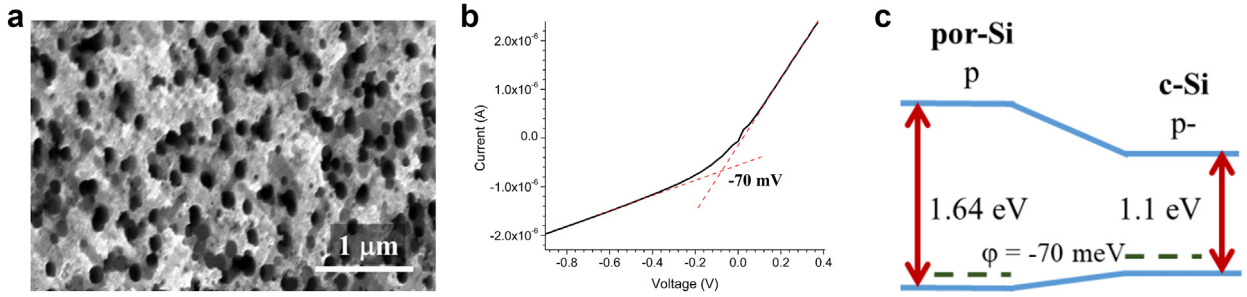

Fig. 2. a) SEM micrograph of a top view of por-Si. b) I–V characteristics of the por-Si/Si structure. c) Energy band diagram of the por-Si/Si structure.

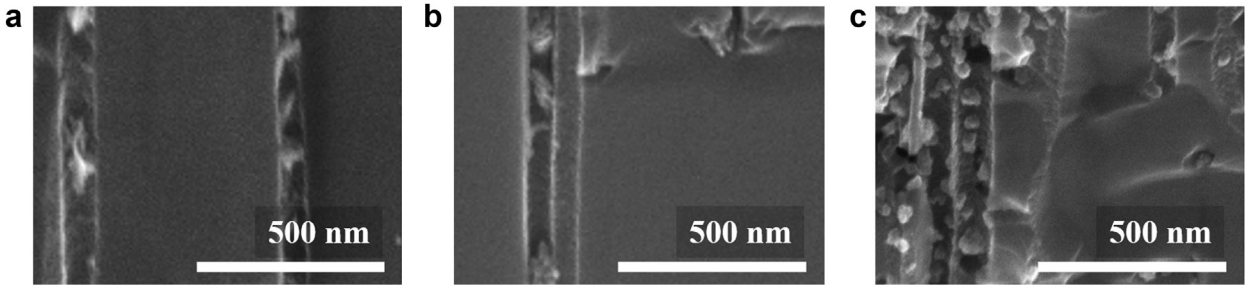

Fig. 3. Cross sectional SEM micrographs of the different TiO_2/por-Si heterostructures: a) "high", b) "medium", and c) "low". The regions between each two parallel vertical lines are the pores in Si, and the spots enclosed in them are TiO_2 particles.

being limited by the reaction rate; thus, there is enough time for the reactant to diffuse into the pores, increasing the spatial density of TiO_2 particles. The morphology of the TiO_2 particles also changed from sample to sample. In the sample "high", the morphology is similar to nanoflakes. In "medium", the flakes are thicker. In "low", the particles seem to be denser and faceted. It is worthy to emphasize that this kind of deposits, covering the pore walls, complex equipment like ALD is commonly used [16,18].

The I–V characteristics of the TiO_2/por-Si heterostructures are shown in Fig. 4. As can be observed, the shape of the curves is very similar to the I–V characteristics of tunnel diodes [28]. A characteristic of the I–V curves of tunnel diodes is a section of negative differential resistance (NDR). However, depending on the heterostructure, this effect can be explained by different models. In a report of a tunnel diode, TiO_2 has been used just as a physical nanometric barrier (deposited by ALD) [29]. In the present case, the tunneling barrier is formed by the TiO_2/por–Si junction. To be able to explain the tunneling process, it is simpler considering the band diagrams of the heterojunction (see Fig. 5). For simplicity, the por-Si/c–Si junction is not shown in the band diagrams. This junction does not limit carrier transport, as seen in Fig. 3. Under conditions close to an open circuit and when applying small positive voltages (reverse polarization), the observed current is given by minority carriers (indicated with thin arrows in the diagram of Fig. 5a). As can be observed, the bands bend to reach equilibrium, producing a large barrier of about 1.2 eV for electrons, the majority carriers. TiO_2 is commonly an n-type semiconductor [30,31], with a bandgap of 3.3 eV. The donor level is about 0.4 eV below the conduction band and is given by defects related to oxygen-sites [30]. When direct polarizing (negative voltages, as in Fig. 5b) above the potential barrier, the negative current increases steeply. The thick arrow indicates the current of majority carriers. On the other hand, when we reverse polarizing at potentials much larger than the bandgap of por-Si, the electrons can tunnel through the barriers ballistically (see Fig. 5c), competing with the current of minority carriers. The tunneling current is not high because the materials are not highly doped, and consequently, the barrier is not so narrow; however, it is high enough to compete and cause a decrease of the overall current, producing NDR.

3.3. *Temporal oscillations*

A test was made at a constant voltage of 5 V (the voltage in the range of the tunneling effect), recording the current response vs time. With this test, temporal oscillations were obtained from all the samples, as shown in Fig. 6. Surprisingly, the oscillations are fully periodic after a stabilization time. The oscillation

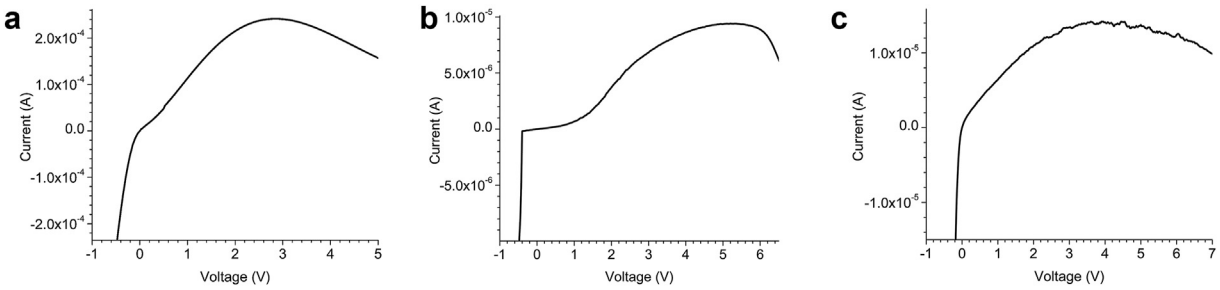

Fig. 4. I–V curves of the different TiO_2/por-Si heterostructures: a) "high", b) "medium", and c) "low".

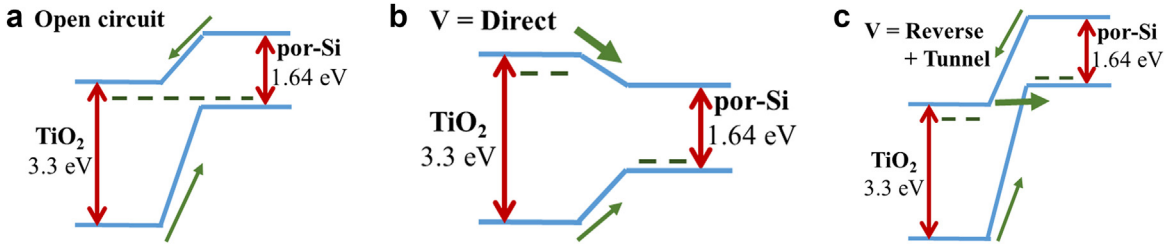

Fig. 5. Band diagrams of the TiO_2/por-Si heterostructures under different external voltages: a) close to open circuit conditions, b) direct polarization, at voltages larger than the energy barrier for electrons, and c) reverse polarization at the voltage of tunneling effect. The thick arrows represent currents of majority carriers, while the thin arrows represent currents of minority carriers.

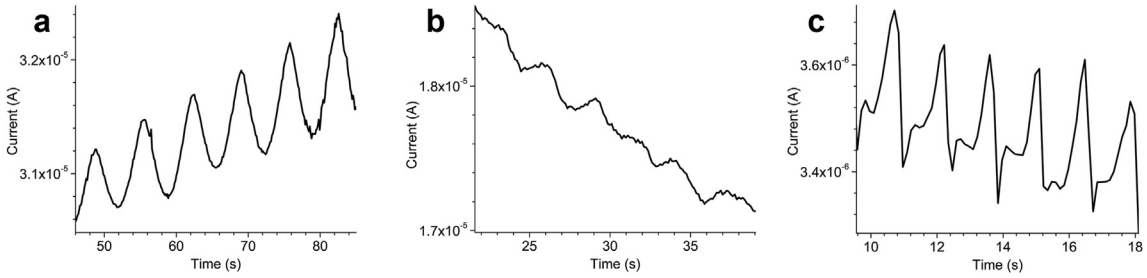

Fig. 6. I-t curves of the different TiO_2/por-Si heterostructures of this work, recorded applying 5V: a) "high", b) "medium", and c) "low".

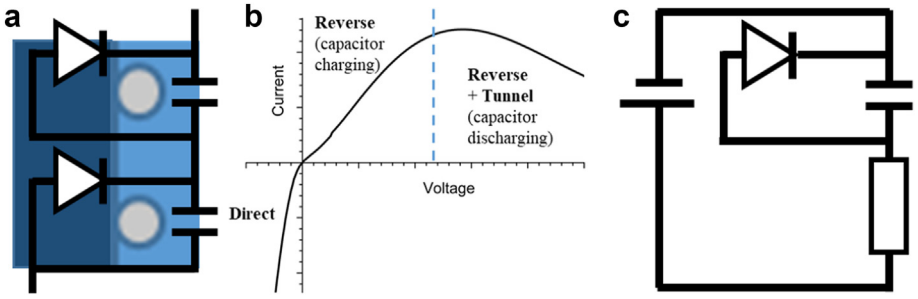

Fig. 7. a) Schematic of the interface between TiO_2 particles (circles) and Si pore walls, with their corresponding electrical model. b) Typical I–V curve of the TiO_2/por-Si heterostructures, indicating the charging/discharging of the capacitors of a). c) Simplified electrical model of the complete TiO_2/por-Si devices, with external voltage source.

frequency is of around 0.16 Hz for "high", 0.3 Hz for "medium", and 0.71 Hz for "low". These values were obtained by calculating the FFT of the curves after the stabilization time. These results correlate well with the spatial density of TiO_2 particles in the pores of por-Si and their contact with the pore walls. The capacitance C associated with the particles is inversely proportional to the coverage level, thus $C_{low} < C_{medium} < C_{high}$. The product of C with the transport resistance R, gives the relaxation time ($t = RC$). The oscillation frequency f is inverse proportional to the relaxation time, thus $f_{low} > f_{medium} > f_{high}$, which agrees with the tendency of the calculated frequency values. The stabilization times, obtained by visual inspection of the I-t curves, are 44.8 s for "high", 21.6 s for "medium", and 9.6 s for "low", representing 2 to 3 oscillations.

Figure 7a shows a representation of a couple of TiO_2 particles attached to a pore wall, together with an electrical model of the system's physical elements. As is evidenced with the I–V curves, the TiO_2/por-Si interface represents a junction that can be modeled with a rectifying diode. On the other hand, the dielectric characteristics of the TiO_2 particles give rise to a capacitance. That capacitance should be charged and discharged during the recording of the I–V curves, as indicated the Fig. 7b. An important fact of capacitors is that they store charges, and the local voltage depends on the amount of stored charge.

Furthermore, the diode's voltage is the same as the one of the capacitor, since they are connected in parallel (see Fig. 7a). As soon as the diode is in the tunneling mode (the capacitor reaches the voltage for the tunneling effect) and the current starts flowing in the opposite direction, the capacitor starts to discharge, and this produces that the local voltage decreases, causing that the diode is not in the tunneling mode anymore. When the diode is not in the tunneling mode, the capacitor charges again, until reaching the tunneling voltage. This process repeats undefined number of times, and it is observable as the temporal oscillations of Fig. 6. The complete simplified electrical model for the whole system, including the external voltage source, is depicted in Fig. 7c. Such a circuit (with the effect previously described) is known as "relaxation oscillator", if the diode presents a trigger voltage (as is the case of tunnel and zener diodes, vacuum bulbs, and neon lamps) [32,33]. The TiO_2/por-Si heterostructure investigated in this work may be the simplest relaxation oscillator ever reported, and it is the first report of using TiO_2 or TiO_2 with Si.

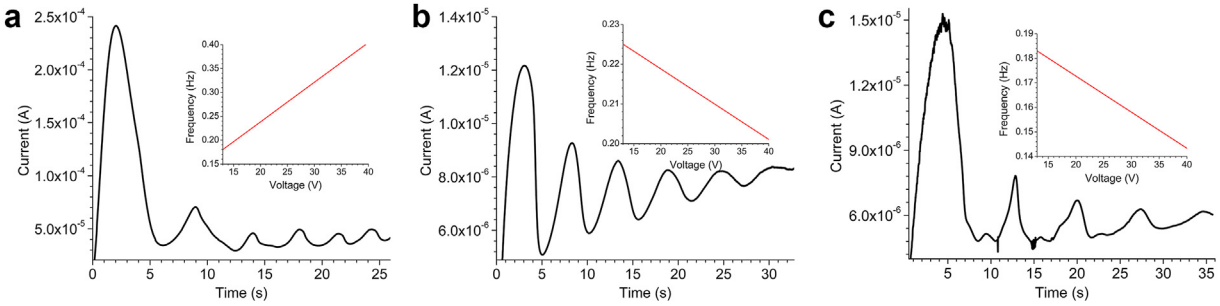

Fig. 8. I-t curves of the different TiO_2/por-Si heterostructures, calculated out of I–V curves: a) "high", b) "medium", and c) "low". The insets indicate the variation of the frequency of the oscillations with respect to voltage.

3.4. Voltage-dependent oscillations

When recording the I–V curves of the heterostructures, oscillations were also obtained. To compare these oscillations with the ones of Fig. 6, the x-axis was converted to time, considering that the voltage sweep rate was constant (1.4 V/s). The resulting curves are shown in Fig. 8. As can be observed, the period of the oscillations changes with time, and their intensity suffers damping. The frequency of oscillations was calculated from cycle to cycle and was plotted vs voltage (as it is known that the parameter that changes with the time when measuring I–V curves is the voltage); these new curves are shown in the insets of Fig. 8. As can be observed, the frequency does not change considerably for samples "medium" and "low", but it doubles for "high" when moving from 13 to 40 V. This can be explained considering that the TiO_2 particles are defect-rich, due to their flake-like shape. In such a case, the exponential factor of the conductivity depends not only on the activation energy and temperature but also on the electric field (i.e., on the applied voltage) [34]. According to this, varying the applied voltage may vary the tunneling voltage and current densities in sample "high"; thus, its oscillation frequency varies with voltage. However, the oscillation frequency at low voltages coincides with the oscillation frequency obtained at constant voltage (Fig. 6). In the case of the samples "medium" and "low", the observed frequency is smaller, and does not vary much with voltage. In those samples the frequency may be limited by the voltage sweep rate that is slower than their characteristic oscillation frequency (determined at constant voltage).

4. Conclusion

This work has demonstrated the formation of TiO_2/por-Si heterostructures with relevant electronic effects by using efficient but simple synthetic methods. TiO_2 nanoparticles decorate the pore walls of por-Si. The sizes of the particles and pore wall coverage depend on the concentration of the precursor for TiO_2.

The current–voltage characteristics of the TiO_2/por-Si heterostructure show that the heterostructure conducts electricity in both polarizations, in contrast to a typical rectifying diode. The shape of these curves is tunnel diode -like. The negative differential resistance (NDR) observed in these TiO_2/por-Si heterostructures has been explained by means of a band diagram considering the flow of minority carriers and their competition with majority carriers that tunnel the heterostructure's interface.

The oscillations found in these heterostructures are periodic, with a characteristic frequency. Moreover, these oscillations have been explained by effects of charge and discharge of a capacitor connected in parallel with a diode (in the tunneling mode), as for the case of relaxation oscillators. Finally, it has been observed that the frequency of the relaxation oscillations presented in this work can be modulated by varying the applied voltage.

Declaration of competing interest

The authors declare that they have no known competing financial interests or personal relationships that could have appeared to influence the work reported in this paper.

Acknowledgements

The authors thank the support of VIEP, BUAP through the project 100523072-VIEP2019. A. Garzon-Roman appreciates the support of CONACyT through a scholarship for graduate studies.

References

[1] I. Iatsunskyi, M. Jancelewicz, G. Nowaczyk, M. Kempiński, B. Peplińska, M. Jarek, K. Załęski, S. Jurga, V. Smyntyna, Atomic layer deposition TiO_2 coated porous silicon surface: structural characterization and morphological features, Thin Solid Films 589 (2015) 303–308, https://doi.org/10.1016/j.tsf.2015.05.056.
[2] P. Kuppusami, N. Parvathavarthini, E. Mohandas, Pulsed laser deposition of anatase and rutile TiO_2 thin films, Surf. Coating. Technol. 201 (2007) 7713–7719, https://doi.org/10.1016/j.surfcoat.2007.03.004.
[3] A. Lotnyk, S. Senz, D. Hesse, Epitaxial growth of TiO_2 thin films on $SrTiO_3$, $LaAlO_3$ and yttria-stabilized zirconia substrates by electron beam evaporation, Thin Solid Films 515 (2007) 3439–3447, https://doi.org/10.1016/j.tsf.2006.10.106.
[4] M. Abdullaha, S.K. Kamarudina, Titanium dioxide nanotubes (TNT) in energy and environmental applications: an overview, Renew. Sustain. Energy Rev. 76 (2017) 212–225, https://doi.org/10.1016/j.rser.2017.01.057.
[5] X.M. Yan, J. Kang, L. Gao, L. Xiong, P. Mei, Solvothermal synthesis of carbon coated N-doped TiO_2 nanostructures with enhanced visible light catalytic activity, App. Sur. Sci. 15 (2013) 778–783, https://doi.org/10.1016/j.apsusc.2012.11.111.
[6] D. Rafieian, W. Ogieglo, T. Savenije, R.G.H. Lammertink, Controlled formation of anatase and rutile TiO_2 thin films by reactive magnetron sputtering, AIP Adv. 5 (2015) 97168–97174, https://doi.org/10.1063/1.4931925.
[7] C.W. Lai, S. Sreekantan, WO_3 deposited TiO_2 nanotube Arrays by thermal evaporation method for effective photocatalytic activity, J. Eng. Sci. 8 (2012) 39–50.
[8] A. Welte, C. Waldauf, C. Brabec, P.J. Wellmann, Application of optical absorbance for the investigation of electronic and structural properties of sol–gel processed TiO_2 films, Thin Solid Films 516 (2008) 7256–7259, https://doi.org/10.1016/j.tsf.2007.12.025.
[9] M. Ishfaq, M.R. Khan, A. Ali, S. Bhardwaj, C. Cepek, A.S. Bhatti, Optical and electrical characteristics of 17 keV X-rays exposed TiO_2 films and Ag/TiO_2/p-Si MOS device, Mater. Sci. Semicond. Process. 63 (2017) 107–114, https://doi.org/10.1016/j.mssp.2017.02.009.
[10] L. Wei, C. Yu, Q. Zhang, H. Liu, Y. Wang, TiO_2-based heterojunction photocatalysts for photocatalytic reduction of CO_2 into solar fuels, J. Mater. Chem. A. 6 (2018) 22411–22436, https://doi.org/10.1039/C8TA08879A.
[11] G. Sahasrabudhe, S.M. Rupich, J. Jhaveri, A.H. Berg, K. Nagamatsu, G. Man, Y.J. Chabal, A. Kahn, S. Wagner, J.C. Sturm, J. Schwartz, Low temperature synthesis of a TiO_2/Si heterojunction, J. Am. Chem. Soc. 137 (2015) 14842–14845, https://doi.org/10.1021/jacs.5b09750.
[12] T. Ji, Q. Liu, R. Zou, Y. Zhang, L. Wang, L. Sang, M. Liao, J. Hu, Enhanced UV-visible light photodetectors with a TiO_2/Si heterojunction using band engineering, J. Mater. Chem. C. 5 (2017) 12848–12856, https://doi.org/10.1039/C7TC04811D.
[13] G. Santamaría-Juárez, E. Gómez-Barojas, E. Quiroga-González, E. Sánchez-Mora, J.A. Luna-López, Oxidized porous silicon as a non-interfering support for

luminescent dyes, Mesoporous Biomater. 3 (2016) 61–66, https://doi.org/10.1515/mesbi-2016-0008.
[14] E. Quiroga-González, J. Carstensen, C. Glynn, C. O'Dwyer, H. Föll, Pore size modulation in electrochemically etched macroporous p-type silicon monitored by FFT impedance spectroscopy and Raman scattering, Phys. Chem. Chem. Phys. 16 (2014) 255–263, https://doi.org/10.1039/C3CP53600A.
[15] Y.S. Sakhare, S.V. Bhoraskar, V.L. Mathe, A.U. Ubale, Electric field assisted enhanced photo catalytic activities of immobilized nano TiO_2 on porous silicon, Mater. Res. Bull. 59 (2014) 205–213, https://doi.org/10.1016/j.materresbull.2014.07.006.
[16] S. Sampath, P. Maydannik, T. Ivanova, M. Shestakova, T. Homola, A. Bryukvin, M. Sillanpää, R. Nagumothu, V. Alagan, Efficient solar photocatalytic activity of TiO_2 coated nano-porous silicon by atomic layer deposition, Superlattice. Microst. 97 (2016) 155–166, https://doi.org/10.1016/j.spmi.2016.06.004.
[17] Q. Wu, D. Li, Z. Chen, X. Fuzhi, New synthesis of a porous Si/TiO_2 photocatalyst: testing its efficiency and stability under visible light irradiation, Photochem. Photobiol. Sci. 5 (2006) 653–655, https://doi.org/10.1039/B517744H.
[18] R. Liu, W. Li, T. Cai, Y. Deng, Z. Ding, Y. Liu, X. Zhu, X. Wang, J. Liu, B. Liang, T. Zheng, J. Li, TiO_2 nanolayer-enhanced fluorescence for simultaneous multiplex mycotoxin detection by aptamer microarrays on a porous silicon surface, ACS Appl. Mater. Interfaces 10 (2018) 14447–14453, https://doi.org/10.1021/acsami.8b01431.
[19] N. Baran, H. Gebavi, L. Mikac, D. Ristic, M. Gotic, K.A. Syed, M. Ivanda, Sensing properties of oxidized nanostructured silicon surface on vaporized molecules, Sensors 19 (2019) 119–131, https://doi.org/10.3390/s19010119.
[20] S. Oussidhoum, D. Hocine, D. Chaumont, A. Crisbasan, M. Bensidhoum, E. Bourennane, A. Moussi, E. Lesniewska, N. Geoffroy, M.S. Belkaid, Optimization of physicochemical and optical properties of nanocrystalline TiO_2 deposited on porous silicon by metal-organic chemical vapor deposition (MOCVD), Mater. Res. Express 6 (2019) 125917–125924, https://doi.org/10.1088/2053-1591/ab6539.
[21] F.N. Fahrizal, M.K. Ahmad, N.M. Ramli, N. Ahmad, R. Fakhriah, F. Mohamad, N. Nafarizal, C.F. Soon, A.S. Ameruddin, A.B. Faridah, M. Shimomura, K. Murakami, Fabrication of TiO_2 nanostructures on porous silicon for thermoelectric application, AIP Conf. Proc. 1883 (2017) 20031–20039, https://doi.org/10.1063/1.5002049.
[22] A.-H. Chiou, S.-D. Wu, R.-C. Hsiao, C.-Y. Hsu, TiO_2–silicon nanowire arrays for heterojunction diode applications, Thin Solid Films 616 (2016) 116–121, https://doi.org/10.1016/j.tsf.2016.07.039.
[23] A. Garzon-Roman, C. Zuñiga-Islas, E. Quiroga-González, Modulation of morphology and optical characteristics of TiO_2 grown into porous silicon by an easy approach, J. Mater. Sci. Mater. Electron. 30 (2019) 21503–21513, https://doi.org/10.1007/s10854-019-02540-1.
[24] V. Aca-López, E. Quiroga-González, E. Gómez-Barojas, J. Świątowska, J.A. Luna-López, Effects of the doping level in the production of silicon nanowalls by metal assisted chemical etching, Mater. Sci. Semicond. Process. 118 (2020) 105206–105212, https://doi.org/10.1016/j.mssp.2020.105206.
[25] P. Ramesh, C. Suresh Kumar, Studies on gold/porous silicon/crystalline silicon junctions, J. Porous Mater. 7 (2000) 299–301, https://doi.org/10.1023/A:1009604703115.
[26] A. Mortezaali, S. Ramezani Sani, F. Javani Jooni, Correlation between porosity of porous silicon and optoelectronic properties, J. Non-Oxide Glasses 1 (2009) 293–299.
[27] J.T. Frederiksen, P.G. Melcher, E. Veje, Electrical band-gap energy of porous silicon and the band offsets at the porous-silicon/crystalline-silicon heterojunction measured versus sample temperature, Phys. Rev. B 58 (1998) 8020–8024, https://doi.org/10.1103/PhysRevB.58.8020.
[28] L. Esaki, New phenomenon in narrow Germanium p-n junctions, Phys. Rev.Phys. Rev. 109 (1958) 603, https://doi.org/10.1103/PhysRev.109.603.
[29] J.J. Guttman, C.B. Chambers, A. Villagracia, G. Nonato, C. Santos, P.R. Berger, Negative differential resistance in polymer tunnel diodes using atomic layer deposited, TiO_2 tunneling barriers at various deposition temperatures, Org. Electron. 47 (2017) 228–234, https://doi.org/10.1016/j.orgel.2017.05.015.
[30] M.B. Sarkar, A. Mondal, B. Choudhuri, B.K. Mahajan, S. Chakrabartty, C. Ngangbam, Enlarged broad band photodetection using Indium doped TiO2 alloy thin film, J. Alloys Compd. 615 (2014) 440–445, https://doi.org/10.1016/j.jallcom.2014.06.184.
[31] S. Zhao, Y. Chen, Z. Zhao, L. Jiang, C. Zhang, J. Kong, X. Zhu, Enhanced capacitance of TiO_2 nanotubes topped with nanograss by H_3PO_4 soaking and hydrogenation doping Electrochim, Acta 266 (2018) 233–241, https://doi.org/10.1021/acs.langmuir.8b04162.
[32] J.M. Ginoux, C. Letellier, Van der Pol and the history of relaxation oscillations: toward the emergence of a concept, Chaos, An Interdiscipl. J. Nonlin. Sci. 22 (2012) 23120–23156, https://doi.org/10.1063/1.3670008.
[33] J. Nagumo, M. Shimura, Self-oscillation in a transmission line with a tunnel diode, Proc. IRE 49 (1961) 1281–1291, https://doi.org/10.1109/JRPROC.1961.287920.
[34] D. Bozyigit, W.M.M. Lin, N. Yazdani, O. Yarema, V. Wood, A quantitative model for charge carrier transport, trapping and recombination in nanocrystal-based solar cells, Nat. Commun. 6 (2015) 6180–6189, https://doi.org/10.1038/ncomms7180.